SUPPLEMENTARY INFORMATION
https://doi.org/10.1038/s41929-018-0190-6

nature catalysis

In the format provided by the authors and unedited.

Corrected: Author Correction

Bimetallic synergy in cobalt–palladium nanocatalysts for CO oxidation

Cheng Hao Wu[1,2], Chang Liu[3], Dong Su[4], Huolin L. Xin[4], Hai-Tao Fang[2,5], Baran Eren[2], Sen Zhang[3*], Christopher B. Murray[6*] and Miquel B. Salmeron[2,7*]

[1]Department of Chemistry, University of California, Berkeley, Berkeley, CA, USA. [2]Materials Science Division, Lawrence Berkeley National Laboratory, Berkeley, CA, USA. [3]Department of Chemistry, University of Virginia, Charlottesville, Virginia, USA. [4]Center for Functional Nanomaterials, Brookhaven National Laboratory, Upton, New York, USA. [5]School of Materials Science and Engineering, Harbin Institute of Technology, Harbin, China. [6]Department of Chemistry, University of Pennsylvania, Philadelphia, PA, USA. [7]Department of Materials Science and Engineering, University of California, Berkeley, Berkeley, CA, USA. *e-mail: sz3t@virginia.edu; cbmurray@sas.upenn.edu; mbsalmeron@lbl.gov

Supplementary Information

Bimetallic Synergy in Cobalt-Palladium Nanocatalysts for CO Oxidation

Cheng Hao Wu[1,2], Chang Liu[3], Dong Su[4], Huolin L. Xin[4], Hai-Tao Fang[2,5], Baran Eren[2], Sen Zhang[3,*], Christopher B. Murray[6,*], and Miquel Salmeron[2,7,*]

[1] Department of Chemistry, University of California, Berkeley, Berkeley, California 94720, USA

[2] Material Sciences Division, Lawrence Berkeley National Laboratory, Berkeley, California 94720, USA

[3] Department of Chemistry, University of Virginia, Charlottesville, Virginia 22904, USA

[4] Center for Functional Nanomaterials, Brookhaven National Laboratory, Upton, New York 11973, USA

[5] School of Materials Science and Engineering, Harbin Institute of Technology, Harbin, Heilongjiang 150001, China

[6] Department of Chemistry, University of Pennsylvania, Philadelphia, Pennsylvania 19104, USA

[7] Department of Materials Science and Engineering, University of California, Berkeley, Berkeley, California 94703, USA

[*]To whom correspondence should be addressed. Email: sz3t@virginia.edu; cbmurray@sas.upenn.edu; mbsalmeron@lbl.gov.

Supplementary Methods

Process and analysis procedures of XPS spectra

The energy scales of all XPS spectra were calibrated by shifting the Fermi edge positions measured with corresponding photon energy to zero. The Pd*3d* spectra of $Co_{0.38}Pd_{0.62}$ and $Co_{0.52}Pd_{0.48}$ have a rather surprising shift of 0.4-0.5 eV towards lower binding energy as well as drastically different fermi edge line shape, which we cannot fully understand or explain. Because all the elements went through certain chemical changes during the experiments, including Si in the substrate, it is difficult to use the peak of any particular elements as internal calibration reference. Tentatively, we aligned the main peak in Pd*3d* spectra for these two samples with the other three samples. Given the fact that these two samples barely showed changes in the surface composition, such realignment does not affect the validity of our conclusion. Because of slightly different attenuation of 100mTorr CO and 100mTorr O_2, for the purpose of better visual comparison, in the figures where spectra under oxidation/reduction conditions were overlaid, the spectra were normalized at the lower energy end of the spectra.

Pd*3d* XPS spectra were quantitatively analyzed by peak deconvolution using casaXPS software, preceded by subtracting a Shirley-type background. The metallic Pd component was fitted using an asymmetric line shape DS(0.01,175)SGL(30), which was determined by optimizing the fitting results on the fully reduced pure Pd NPs after treated in H_2 at 150°C. The components related to rest of the Pd species, including surface sub-oxide, CO-coordinated Pd, surface PdC_x, and bulk PdO_x, were fitted using line shapes of symmetric SGL functions. Peak fitting was not performed the Pd*3d* spectra of $Co_{0.52}Pd_{0.48}$ NPs because of their low signal-to-noise ratios and relatively unchanged shapes during the entire experiments.

Co*3p*/Pd*4p* spectra was used to estimate the surface Co/Pd ratios. The information depth of these spectra is estimated to ~0.9 nm according to NIST Electron Inelastic-Mean-Free-Path Database (Version 1.2). In-depth analysis of Co oxidation states as well as accurate calculation of the Co/Pd ratios is impossible for multiple reasons, including substantial overlapping of Pd*4p* high energy tails under Co*3p* main peak, the spin-orbital splitting of both elements that cannot be well resolved, as well as the coexistence of multiple Co and Pd species. A crude fitting procedure was performed for the sole purpose of estimating the peak areas, as illustrated in Supplementary Figure 7, preceded by subtracting a linear background, except for $Co_{0.38}Pd_{0.62}$, in which case a Shirley-type background is necessary to avoid negative peak intensity. The Co/Pd ratios were then calculated from the peak areas (PA) of Co*3p* and Pd*4p* signals, ionization cross sections (ICS) of each element at the corresponding incident photon energies, using the following formula:

$$Atomic\ Ratio\ \frac{Co}{Pd} = \frac{PA(Co)}{PA(Pd)} \times \frac{ICS(Pd)@500eV}{ICS(Co)@500eV} \quad (1)$$

Process and analysis procedures of EELS spectra

Raw EELS spectra acquired from ETEM/EELS experiments were processed using the open-source Cornell Spectrum Imager following the method described in the article by R. Hovden et al. (*Microscopy Today 2013, **21**, 40-44*). A power function was used for background subtraction and each spectrum was then normalized by L_3 peak intensity. All spectra in Supplementary Figure 9a were shifted to align the L_3 peak to ~778eV. The areas of L_3 and L_2 peaks were calculated by integrating the spectra under L_3 peak (770eV, 786eV) and under L_2 peak (788eV, 802eV) respectively, preceded by subtracting a linear background within each energy window.

Process and analysis procedures of XAS spectra

The energy scales of all Co L-edge XAS spectra were calibrated by first shifting the L_3 peak of a Co metal foil reference sample to 778.1 eV and then applying the same energy shift to all the subsequently acquired Co L-edge spectra. All XAS spectra were first normalized by the photon flux profile represented by a TEY current collected on a gold mesh in the upstream x-ray pipeline. After a linear background was subtracted from each spectrum based on the slope of the pre-edge region, the spectra were normalized again by setting L_3 peak intensity to 1.

Supplementary Notes

Thickness estimation of CoO_x shell for a $Co_{0.24}Pd_{0.76}$ particle

A back-of-the-envelope calculation of Co shell thickness might help us understand why it is difficult to image these thin Co shells. Assuming all of the Co atoms in the $Co_{0.24}Pd_{0.76}$ particles redistribute uniformly to the surface of 4.5nm sphere (ignore the density difference between Co and Pd) and form a thin shell with thickness of Δr. The percentage of Co can be expressed in the following equation:

$$Co\% = 1 - \frac{Volume\ of\ Pd\ core}{Volume\ of\ entire\ particle} = 1 - \frac{(4.5-\Delta r)^3}{4.5^3} = 0.24 \quad (2)$$

Solve this equation and we get Δr ~ 0.4nm. If all the Co were oxidized to CoO (~40% volume expansion), the CoO_x shell will be less than 0.6nm, about two atomic layers, which will be very challenging to image, even more so in the case of lower Co-content particles and/or under in-situ conditions.

For a larger particle (e.g. 10nm diameter) with the same Co content, solve the same equation and we get Δr ~ 0.9nm. We can expect a ~1.3nm oxide shell after oxidation, which should be much easier to observe in STEM.

If we assume the thickness of a perfect monolayer is ~ 0.3nm, we can also estimate the overall Co percentage in a 4.5nm CoPd particle where the Pd core is covered by a perfect monolayer of Co:

$$Co\% = 1 - \frac{(4.5-0.3)^3}{4.5^3} = 19\% \quad (3)$$

Supplementary Figures

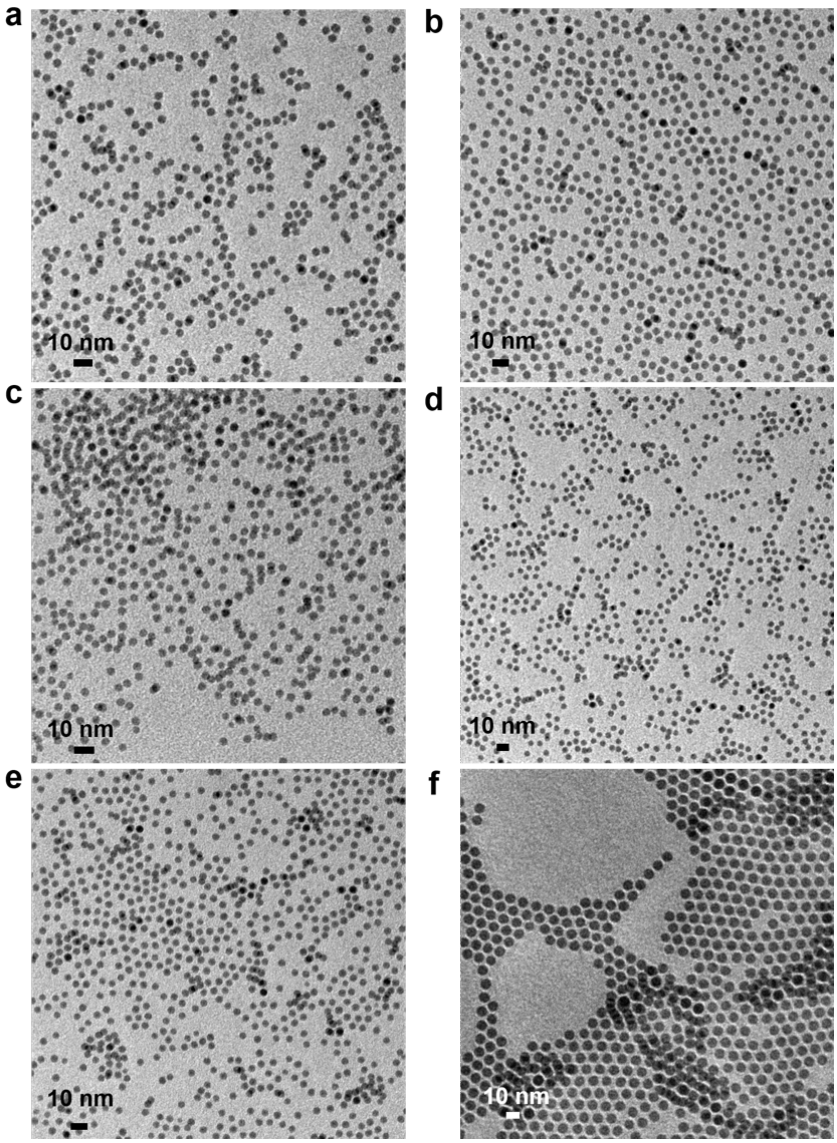

Supplementary Figure 1. (**a**-**e**) TEM image of as-synthesized $Co_{0.10}Pd_{0.90}$ (**a**), $Co_{0.24}Pd_{0.76}$ (**b**), $Co_{0.38}Pd_{0.62}$ (**c**), $Co_{0.52}Pd_{0.48}$ (**d**) and Pd (**e**) NPs in the presence of TBP. (**f**) TEM image of as-synthesized $Co_{0.24}Pd_{0.76}$ NPs in the presence of TOP.

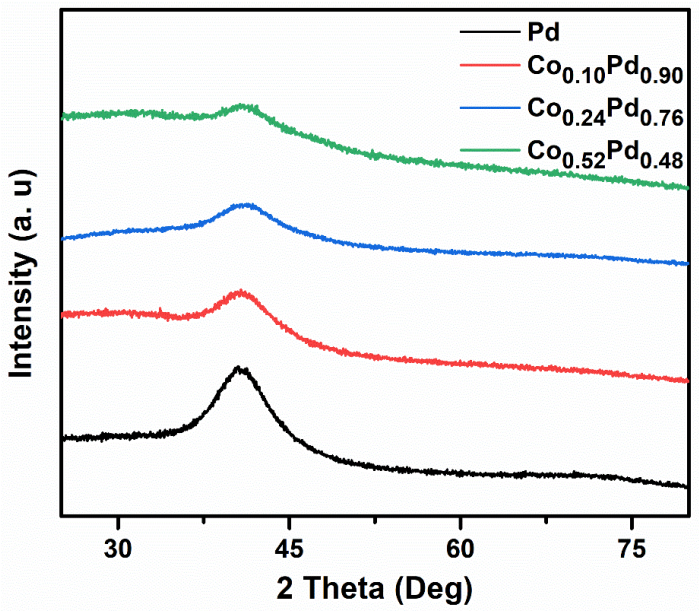

Supplementary Figure 2. XRD patterns of as-synthesized Pd, $Co_{0.10}Pd_{0.90}$, $Co_{0.24}Pd_{0.76}$ and $Co_{0.52}Pd_{0.48}$ NPs.

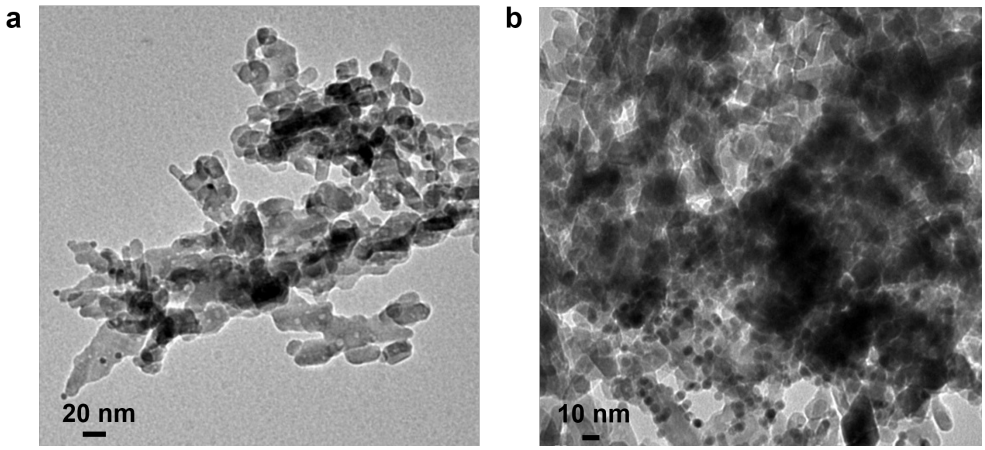

Supplementary Figure 3. TEM image of $Co_{0.24}Pd_{0.76}$ NPs supported on Al_2O_3 before (a) and after (b) pre-treatment (annealed in air at 300 °C for 3 hours).

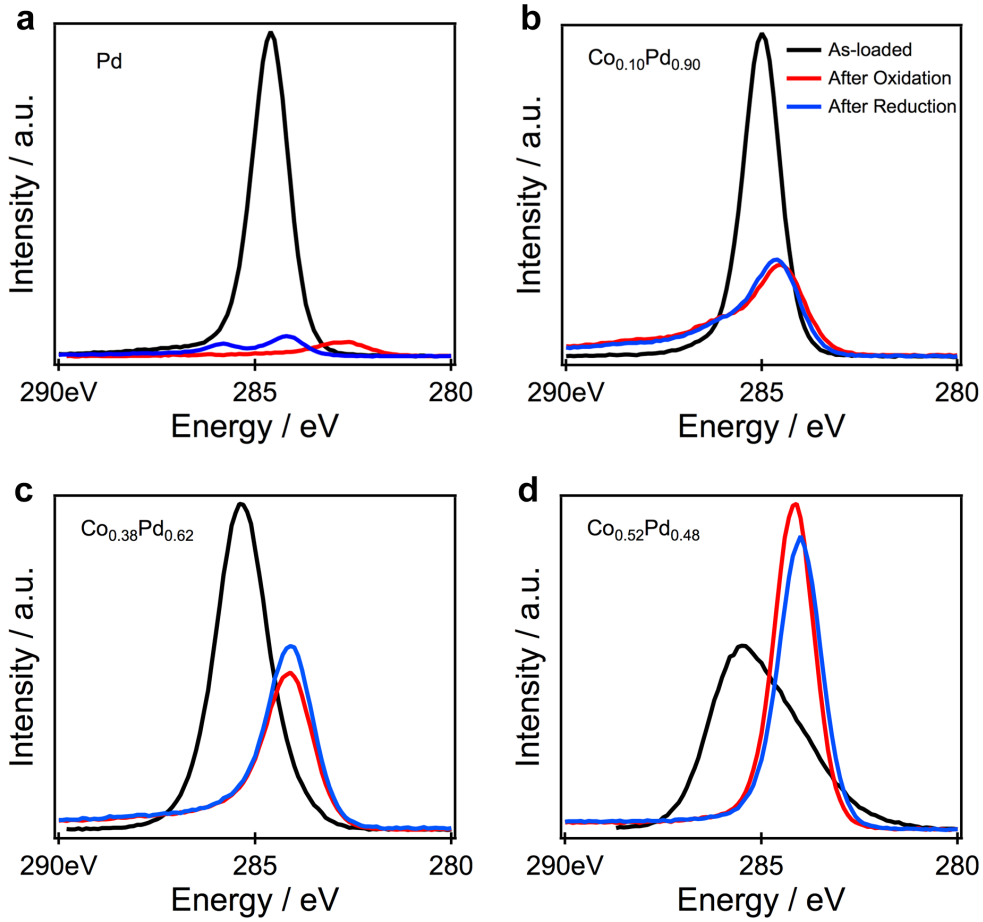

Supplementary Figure 4. C*1s* spectra of (a) Pd, (b) $Co_{0.10}Pd_{0.90}$, (c) $Co_{0.38}Pd_{0.62}$, and (d) $Co_{0.52}Pd_{0.48}$ before and after pre-treatments.

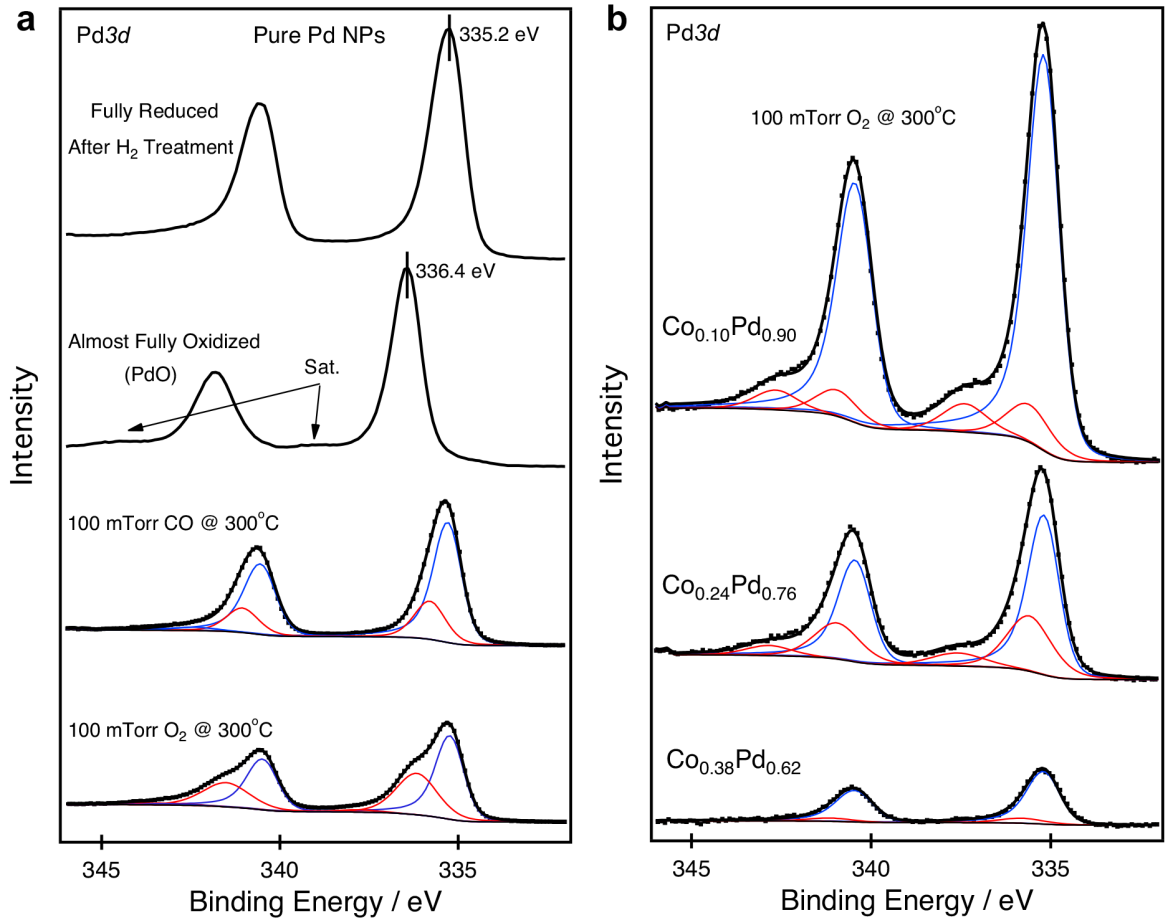

Supplementary Figure 5. (a) Pd*3d* spectra of metallic Pd NPs (fully reduced in H_2) and fully oxidized (in O_2) Pd NPs during the pre-treatments, and deconvoluted Pd*3d* spectra when Pd NPs were exposed to 100 mTorr of CO or O_2 at 300°C. (b) Deconvoluted Pd*3d* spectra of $Co_{0.10}Pd_{0.90}$, $Co_{0.24}Pd_{0.76}$, and $Co_{0.38}Pd_{0.62}$ under 100 mTorr of O_2 at 300°C. Blue components represent metallic Pd; Red components represent oxidized Pd species.

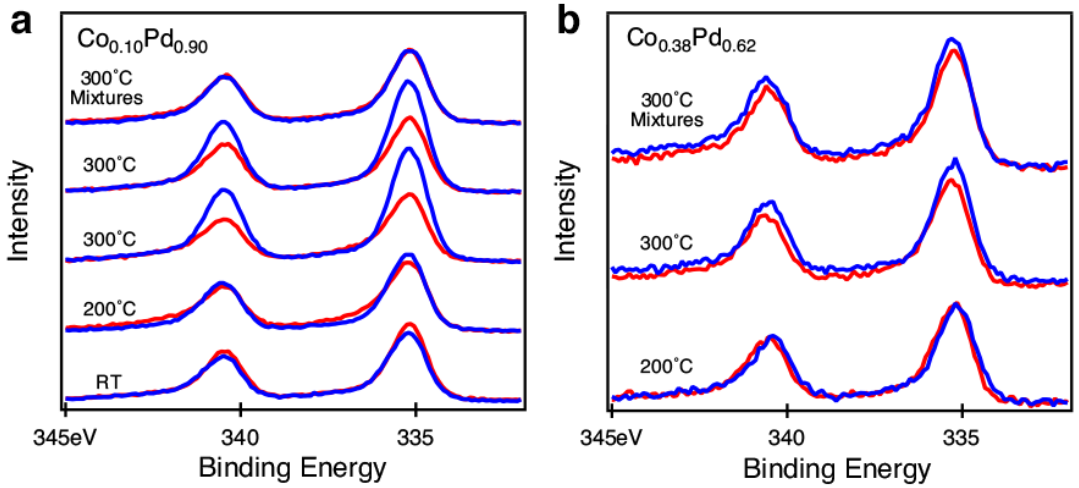

Supplementary Figure 6. Pd*3d* spectra of (a) $Co_{0.10}Pd_{0.90}$ and (b) $Co_{0.38}Pd_{0.62}$ NPs under 100mTorr of CO, O_2, and their mixtures (1:4 or 4:1) at different temperatures. Blue spectra were acquired under CO only or CO rich conditions; Red spectra were acquired under O_2 only or O_2 rich conditions.

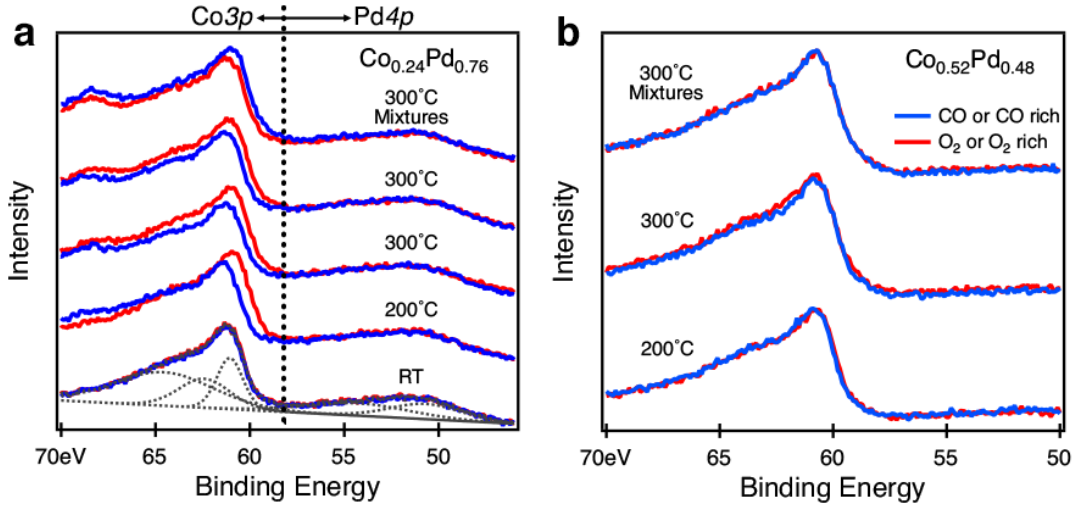

Supplementary Figure 7. Co*3p*/Pd*4p* spectra of (a) $Co_{0.24}Pd_{0.76}$ and (b) $Co_{0.52}Pd_{0.48}$ NPs under 100mTorr of CO, O_2, and their mixtures (1:4 or 4:1) at different temperatures. Blue spectra were acquired under CO only or CO rich conditions; Red spectra were acquired under O_2 only or O_2 rich conditions.

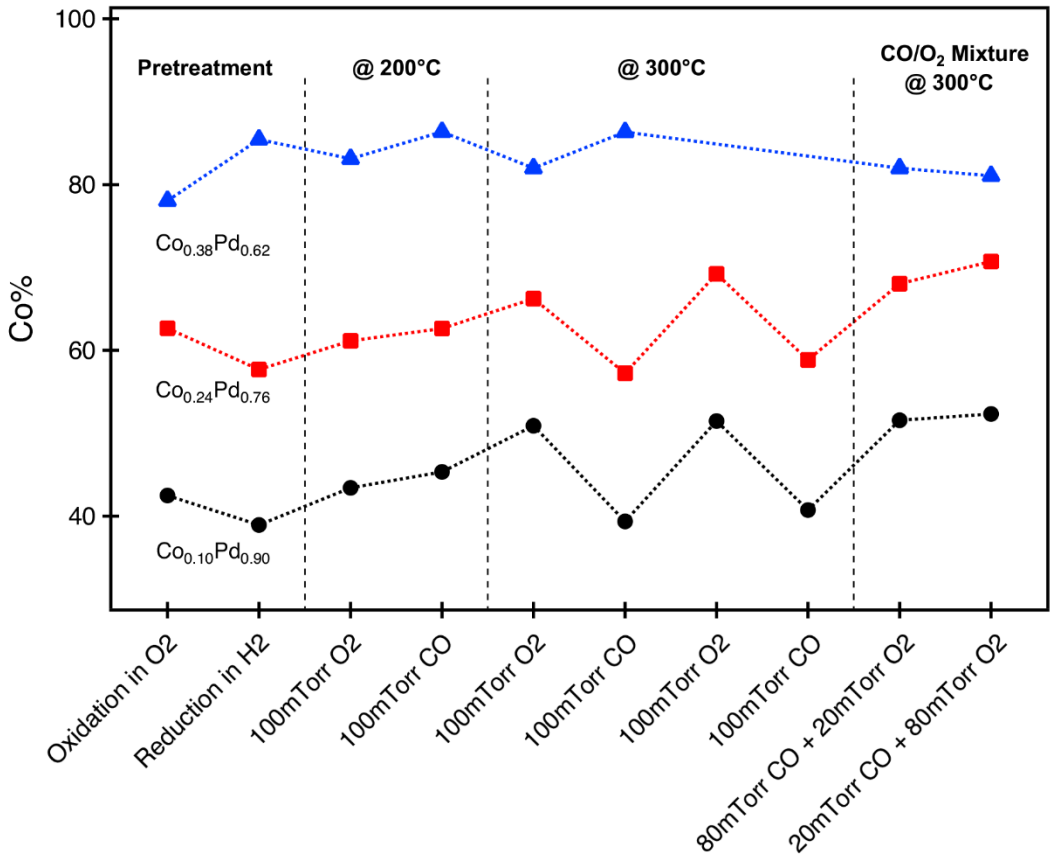

Supplementary Figure 8. Percentage of Co (metal basis) under different conditions, estimated from the peak area ratios in Co*3p*/Pd*4p* spectra for $Co_{0.10}Pd_{0.90}$, $Co_{0.24}Pd_{0.76}$, and $Co_{0.38}Pd_{0.62}$ NPs.

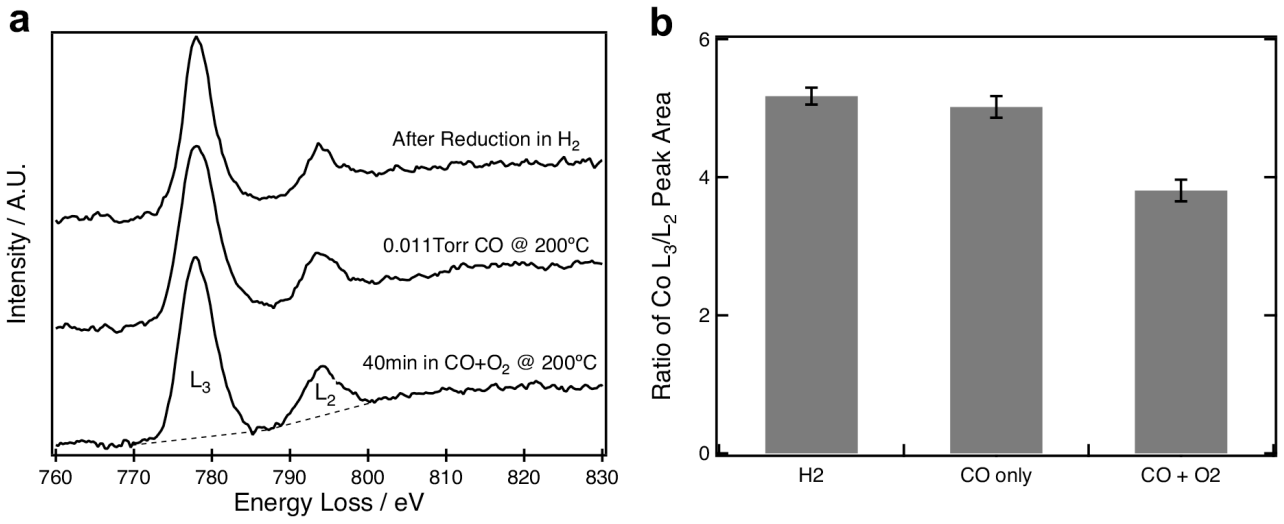

Supplementary Figure 9. (a) Co L-edge EELS spectra acquired after reduction in H_2, while heating in 0.11 Torr CO at 200°C, and after 40min heating in 0.11 Torr CO and 0.44 Torr O_2 at 200°C. (b) Corresponding L_3/L_2 ratios under three different conditions. The error bars included here represent the standard deviation of L_3/L_2 ratios calculated from 3-4 different EELS spectra acquired under identical conditions.

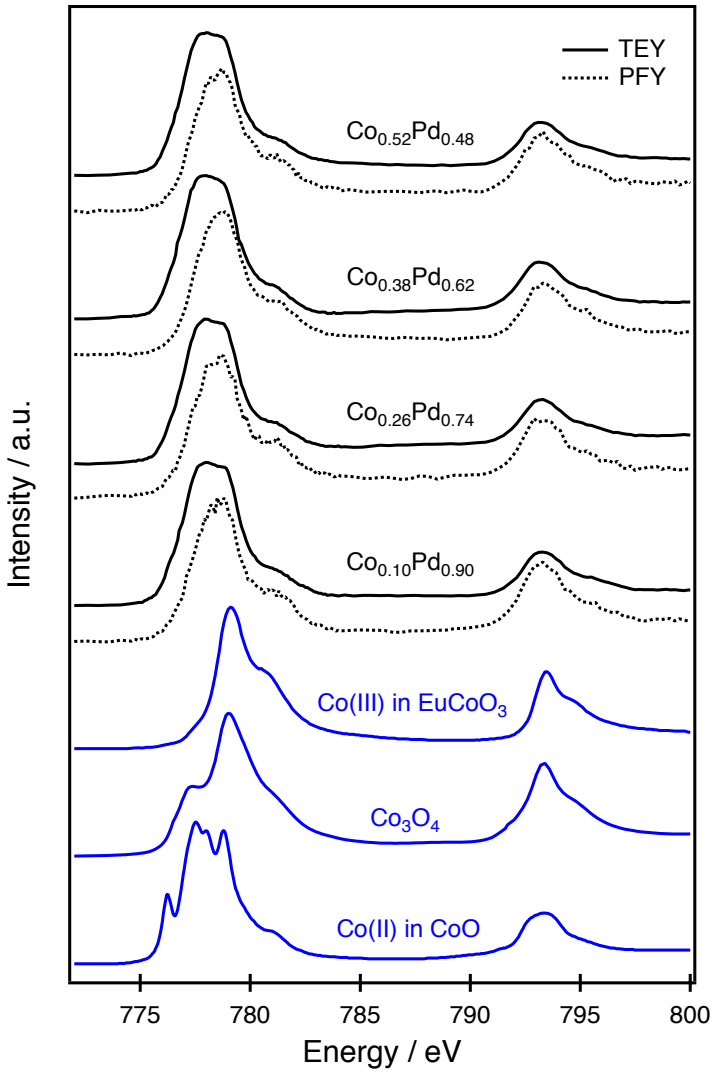

Supplementary Figure 10. *Ex-situ* Co L-edge XAS TEY (solid) and PFY (dotted) spectra of CoPd alloy NPs after APXPS measurements, in comparison with reference spectra of different Co compounds.

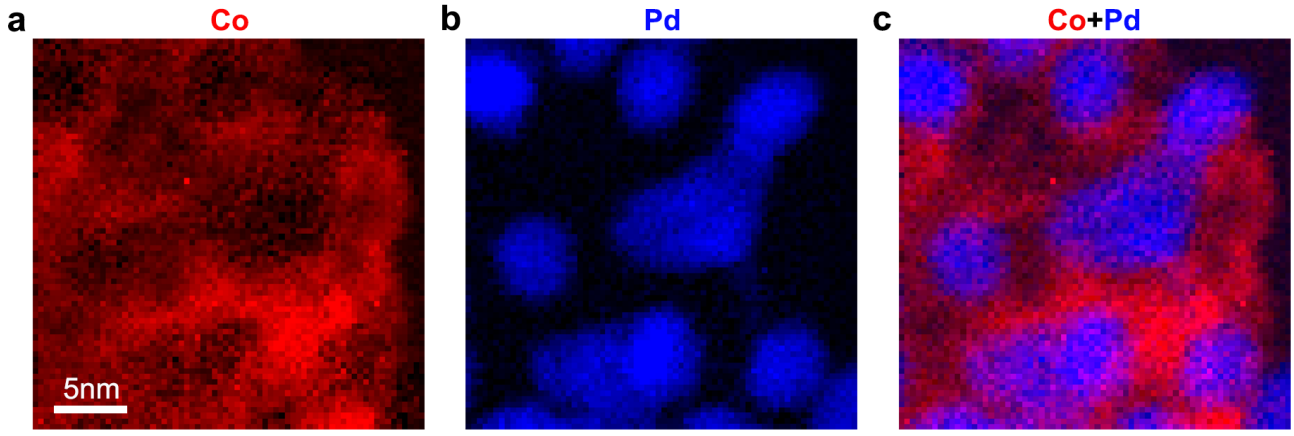

Supplementary Figure 11. Representative STEM-EELS elemental mapping of Co (a), Pd (b), and overlaid Co+Pd (c) of $Co_{0.52}Pd_{0.48}$ NPs (supported on carbon) after pre-treatment.

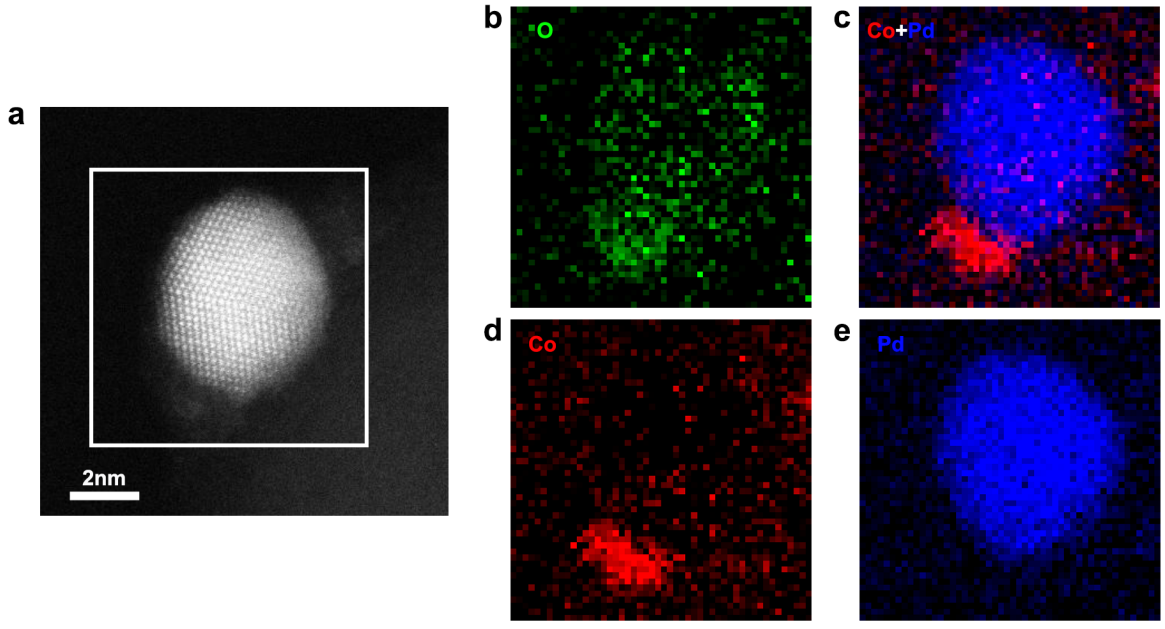

Supplementary Figure 12. STEM and EELS elemental mapping of pre-treated 4.5nm $Co_{0.24}Pd_{0.76}$ NPs. (a), Representative dark-field STEM image of $Co_{0.24}Pd_{0.76}$ NPs. O (b), overlaid Co+Pd (c), Co (d), and Pd (e) EELS mapping of the NP.